Si *et al.*
Chinese Journal of Mechanical Engineering (2022) 35:146
https://doi.org/10.1186/s10033-022-00820-2

Chinese Journal of Mechanical Engineering

ORIGINAL ARTICLE

Open Access

Principle and Control of Active Engine Mount Based on Magnetostrictive Actuator

Zhiyuan Si[1,2], Xianxu 'Frank' Bai[1*], Lijun Qian[1] and Peng Chen[3]

Abstract

Engine mount system affects the automobile NVH performance. Active mounts would achieve excellent vibration isolation and relative displacement control performance in a broad frequency bandwidth by outputting controlled force to the mounting system. The actuator and control method of the active mounts determine the system performance. In this paper, an active mount based on the smart material, i.e., Terfenol-D rod, is proposed, which mainly includes three parts: rubber spring, magnetostrictive actuator (MA), and hydraulic amplification mechanism (HAM). Dynamic model of the active mount is correspondingly established. A state feedback control method based on *x*-LMS (Least-Mean-Square) algorithm is proposed as well. Specifically, with the consideration of the unmeasurable state parameters in the active mounting system, an *x*-LMS state feedback controller with the system state as the reference signal is constructed by employing Sage-Husa Kalman filter to realize the state estimation of the active mounting system. Then a detailed analysis of the proposed control method is conducted, with deriving iterative formula of tap-weight vector. Sequentially, the problem of the dependence on the excitation signal in the *x*-LMS algorithm is addressed. The feasibility and capability of the proposed control method are verified and evaluated by simulation of a two-degree-of-freedom active mounting system.

Keywords: Terfenol-D rod, *x*-LMS, Sage-Husa Kalman filter, Semi-active control, Active mount controller

1 Introduction

Engine mount system plays an important role in reducing the transmission of engine vibration to the body and improving the NVH characteristics of the vehicle [1]. However, the trend of increased engine power combined with lighter vehicle frames poses vibration isolation problems which passive mounts alone cannot adequately address. Moreover, it is difficult for passive mounts to meet the requirements of vibration isolation and relative position control performance in the wide frequency band simultaneously [2]. Active mounts can achieve better vibration isolation and relative displacement control performance in a broader frequency bandwidth via active force [3–5]. In the research of active mounting systems, the actuators and control methods that directly affect system performance have received extensive attention [6–17].

Active mount actuators are mainly divided into two categories: One is the electromagnetic actuator [9, 11, 16]. The characteristics of the electromagnetic actuator itself limit the bandwidth of the active mount (<80 Hz) [7]. The other is the smart material-based actuators. Thanks to the broadband response characteristics of smart materials, such active mounts with broad frequency bandwidth attract much attention [7, 8, 10, 18, 19]. Since smart materials produce a stroke below mount requirements, the implementation of these materials in active mounts requires stroke amplification [20]. Mechanical amplification based on stacking or levers typically is too bulky to be used in engine mount. Hydraulic amplification would be more suitable for engine mount design, which use pistons of different areas with the smart material driving

*Correspondence: bai@hfut.edu.cn

[1] Laboratory for Adaptive Structures and Intelligent Systems (LASIS), Department of Vehicle Engineering, Hefei University of Technology, Hefei 230009, China
Full list of author information is available at the end of the article

the large piston and the power output delivered by the smaller driven piston. In Refs. [18, 21], the combination of piezoelectric actuator and hydraulic amplification mechanism is used in the design of engine mount. An actuator with magnetostrictive material - Terfenol-D rod and hydraulic amplification mechanism combined with hydraulic passive engine mount form a composite active engine mount in Ref. [7].

Hillis [9] explored x-LMS algorithm with real-time estimation of excitation signal by engine speed to reduce the transmission rate of the electromagnetic-hydraulic active mount. The simulation and experimental results show that the active mounting system based on x-LMS algorithm can effectively reduce its transmission rate. Li et al. [12] designed a hierarchical fuzzy controller for a semi-active mounting system using magnetorheological fluid suspension. Simulation and experimental results verify the feasibility of the hierarchical fuzzy control algorithm in the application of suspension control. Phu et al. [13] explored an adaptive Fuzzy-Sliding Mode control algorithm to control the relative displacement of engine vibration and simulated the vibration isolation performance of ship engine mount system. In addition, the frequency domain control algorithm [22], Skyhook control [23], LQG (Linear Quadratic Gaussian) [24] and H∞ [25, 26] control algorithms, etc. were used in mount control. It should be pointed out that the optimal control based on random disturbance hypothesis [12, 25] take compromise treatment between low-frequency relative displacement control and high-frequency vibration isolation performance in principle. The feedforward x-LMS algorithm can achieve optimal control within the whole frequency range theoretically. However, it is limited by the fact that the engine excitation signal cannot be measured in practical applications.

In this paper, an active mount, with a smart material—Terfenol-D rod-based MA as driving element, is proposed, and its dynamic model is also established. Then, aiming at the problem of the dependence on the excitation signal in the x-LMS algorithm, an x-LMS algorithm with state feedback control method of the active mounting system is proposed by employing Sage-Husa Kalman filter to realize the state estimation. Then a detailed analysis of the proposed control method is conducted. With the output force of a MA as input, the simulation of the transmitted force and relative displacement of the two-degree-of-freedom active mounting system is carried out to verify the proposed control method under different engine conditions (steady and dynamic state).

2 Two-Degree-of-Freedom Mounting System Model

The model of the two-degree-of-freedom active mounting system is shown in Figure 1, the corresponding dynamic state equation can be expressed as

$$\dot{X} = AX + B_1 F_c + B_2 F_{in}, \tag{1a}$$

$$e = CX + DF_c + \eta, \tag{1b}$$

$$A = \begin{bmatrix} 0 & 1 & 0 & 0 \\ \frac{-k_m}{m_e} & \frac{-b_m}{m_e} & \frac{k_m}{m_e} & \frac{b_m}{m_e} \\ 0 & 0 & 0 & 1 \\ \frac{k_m}{m_b} & \frac{b_m}{m_b} & \frac{-(k_s+k_m)}{m_b} & \frac{-(b_m+b_s)}{m_b} \end{bmatrix}, B_1 = \begin{bmatrix} 0 \\ \frac{1}{m_e} \\ 0 \\ -\frac{1}{m_b} \end{bmatrix}, B_2 = \begin{bmatrix} 0 \\ \frac{1}{m_e} \\ 0 \\ 0 \end{bmatrix}, C = \begin{bmatrix} 1 & 0 & -1 & 0 \\ k_m & b_m & -k_m & -b_m \end{bmatrix}, D = \begin{bmatrix} 0 \\ -1 \end{bmatrix}, \tag{1c}$$

where the state variables $X = [x_1\ \dot{x}_1\ x_2\ \dot{x}_2]^T$; m_e and m_b represent a quarter of the engine mass and sprung mass, respectively; k_s and b_s are the suspension stiffness and damping, respectively; k_m and b_m are the stiffness and damping of the engine mount, respectively; F_{in} is vertical excitation force caused by the engine, which is the excitation source of the system; η is $n \times 1$ order measurement noise; x_1, x_2, $\dot{x}_1$ and $\dot{x}_2$ are the displacements of the engine and the sprung mass, and their derivatives with respect to time, respectively; F_c represents the active control force of the mount; residual vibration is represented by the relative displacement and transmitted force between the engine and sprung mass.

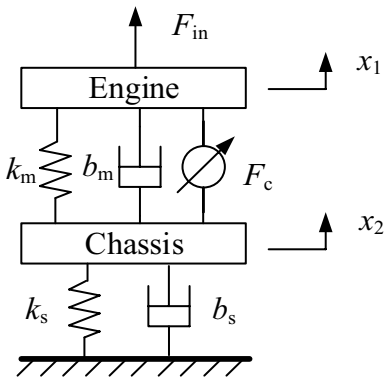

Figure 1 Two-degree-of-freedom active mounting system model

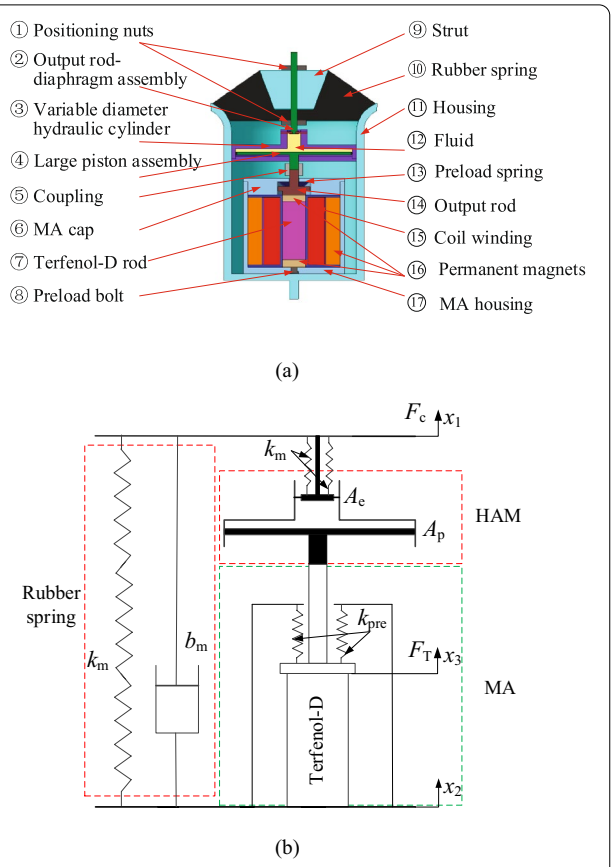

Figure 2 The proposed active mount: **a** configuration and **b** principle

3 Structure of Active Mount Based on MA

The proposed active mount based on MA is shown in Figure 2, which mainly includes three parts: rubber spring, MA and HAM. The rubber spring supports the engine weight, playing the role of the passive mount. The MA outputs active control force, the structure of which includes ⑥ MA cap, ⑦ Terfenol-D rod, ⑧ Preload bolt, ⑬ Preload spring, ⑭ Output rod, ⑮ Coil winding, ⑯ Permanent magnets and ⑰ MA housing. The HAM amplifies the output displacement of the MA, transmits the output force from the MA to the engine, and alleviates the impact on the MA during the engine vibration, which includes ②Output rod-diaphragm assembly, ③Variable diameter hydraulic cylinder ④ Large piston assembly. The output rod-diaphragm assembly of the HAM is connected to ⑨ Strut, and its forced state is adjusted by the upper and lower ① Positioning nuts, and the large piston rod is connected to the output rod of the MA through ⑤ Coupling.

3.1 Model of the Hydraulic Amplification Mechanism

Assuming no compliance of the fluid, then the gain of the hydraulic amplification mechanism can be expressed as [27]

$$K_{\text{amp}} = \frac{A_{\text{p}}}{A_{\text{e}}}, \tag{2}$$

where A_{p} and A_{e} represents effective cross-sectional areas of large and small ends of hydraulic cylinder respectively.

3.2 Model of the MA

The linear constitutive magnetomechanical relations for the Terfenol-D rod along the axial direction is written as [28]

$$\varepsilon = \frac{\sigma}{E^H} + dH, \tag{3a}$$

$$B = d^*\sigma + \mu^\sigma H, \tag{3b}$$

where ε and σ represent Terfenol-D rod axial strain and stress respectively; E^H is the mechanical compliance at constant applied magnetic-field strength H; B is the magnetic-flux within the material. μ^σ is the magnetic permeability at a constant stress; d and d^* are the linear piezomagnetic cross-coupling coefficients. If the magnetostrictive process is assumed to be reversible, then $d^* = d$. This would be normally true for low-level driving forces or fields.

Based on Eq. (3a), with the consideration of the quality and damping effect of the Terfenol-D rod [29–31], we can get

$$\varepsilon = \frac{\sigma}{E^H} + dH - \frac{c_{\text{D}}}{E^H}\dot{\varepsilon} - \frac{\rho l_{\text{T}}^2}{3E^H}\ddot{\varepsilon}, \tag{4}$$

where ρ, l_{T} and c_{D} are the density, length, and internal damping coefficient of the Terfenol-D rod, respectively.

Then, the output force of the Terfenol-D rod is expressed as

$$F_{\text{T}} = -\sigma A_{\text{T}} = E^H A_{\text{T}} dH - E^H A_{\text{T}}\varepsilon - \frac{c_{\text{D}} A_{\text{T}}}{E^H}\dot{\varepsilon} - \frac{\rho l_{\text{T}}^2 A_{\text{T}}}{3E^H}\ddot{\varepsilon}, \tag{5}$$

where A_{T} represents the cross-sectional area of the Terfenol-D rod.

The current flowing in the coil winding and generating the magnetic field H can be calculated through the circuitation of the magnetic field itself

$$H = \frac{nI}{l_{\text{T}}}, \tag{6}$$

where n is the number of turns of the coil winding; I is current flowing in the coil winding.

Substituting $\varepsilon = \frac{x_3}{l_T}$ into Eq. (5), we get

$$F_T = -\sigma A_T = E^H A_T d H - k_T x_3 - b_T \dot{x}_3 - m_T \ddot{x}_3, \tag{7}$$

where $k_T = \frac{E^H A_T}{l_T}$, $b_T = \frac{c_D A_T}{E^H l_T}$, $m_T = \frac{\rho l_T^2 A_T}{3E^H l_T}$.

According to Newton's second law, a dynamic equation is established for the output rod of the MA and the large piston of the HAM

$$m\ddot{x}_3 + k_{pre} x_3 = F_T - K_{amp} F_c - \sigma_p A_T - F_r, \tag{8}$$

where $m = m_r + m_p$, m_r and m_p are the masses of the output rod of the MA and the large piston of the HAM, respectively; k_{pre} is the stiffness of the preloaded spring; σ_p and F_c are prestress and control force (output force of the MA) respectively; F_r is the friction force at the large piston of the HAM, F_r can be quantified using the LuGre model [32], which describes the frictional force based on the bristle interpretation of friction. The LuGre model equations are given by

$$\begin{cases} \frac{dz}{dt} = v - \sigma_0 \frac{|v|}{g(v)} z, \\ g(v) = F_k + (F_s - F_k) e^{-(\frac{v}{v_s})^2}, \\ \sigma_1(v) = \sigma_1 e^{-(\frac{v}{v_d})^2}, \\ F_r = \sigma_0 z + \sigma_1(v) \frac{dz}{dt} + \sigma_2 v, \end{cases} \tag{9}$$

where z is the average bristle deflection; F_s and F_k are the static and coulomb frictional forces; σ_0, σ_1 and σ_2 are the bristle stiffness, bristle damping and viscous damping coefficient respectively. Parameter v_s is the Stribeck velocity and v_d is an additional parameter which controls the velocity dependence of $\sigma_1(v)$.

Combining Eqs. (6), (7) and (8), the control force can be given by

$$F_c = (E^H A_T d \frac{nI}{l_T} - k_a x_3 - b_T \dot{x}_3 - m_a \ddot{x}_3 - \sigma_p A_T - F_r)/K_{amp}, \tag{10}$$

where $k_a = k_T + k_{pre}$, $m_a = m_T + m_r + m_p$.

During the motion of the system, the output displacements of the MA, the engine and the sprung mass meet the following relationship

$$x_3 = \frac{x_1 - x_2}{K_{amp}}. \tag{11}$$

Substituting Eq. (11) into Eq. (10), Eq. (10) can be rewritten as

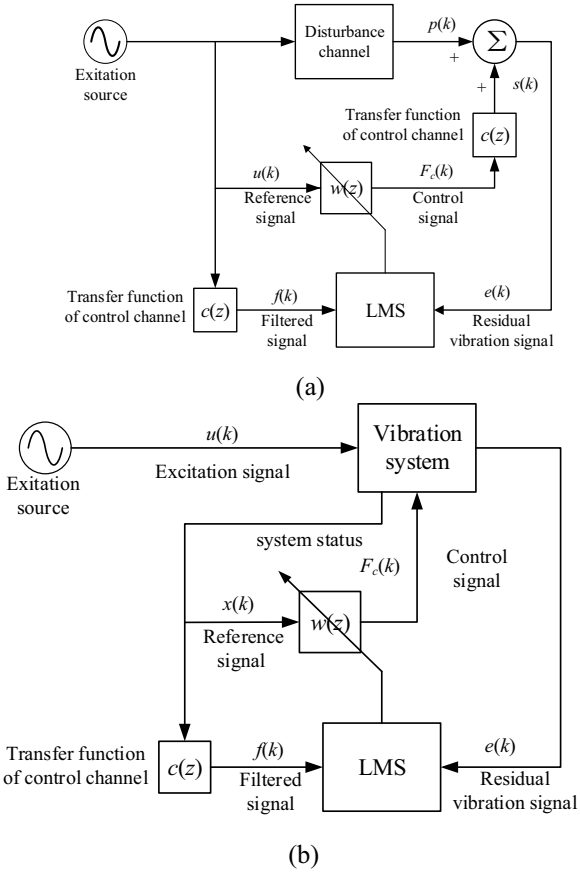

Figure 3 The control diagram: **a** *x*-LMS algorithm [9] and **b** *x*-LMS algorithm with state feedback

$$F_c = (E^H A_T d \frac{nI}{l_T} - k_a \frac{x_1 - x_2}{K_{amp}} - b_T \frac{\dot{x}_1 - \dot{x}_2}{K_{amp}} - m_a \frac{\ddot{x}_1 - \ddot{x}_2}{K_{amp}} - \sigma_p A_T - F_r)/K_{amp}. \tag{12}$$

4 Controller Design

4.1 *x*-LMS Algorithm with State Feedback

X-LMS algorithm as a kind of feedforward control method is widely used in active structural vibration control due to its small calculation amount, easy implementation and strong adaptive ability. The control diagram of *x*-LMS algorithm is shown in Figure 3a, the excitation signal is selected as the filter reference signal $u(k)$, which limits the application of *x*-LMS algorithm when the excitation signal is unmeasurable. Therefore, a solution is proposed to use the system state as the reference signal, the control diagram of the corresponding *x*-LMS algorithm with state feedback is shown in Figure 3b.

In a discrete system, the system state equation can be expressed as

$$X_k = GX_{k-1} + H_1F_{c.k-1} + H_2u_{k-1}, \tag{13a}$$

$$e_k = CX_k + DF_{c.k}, \tag{13b}$$

where X_k represents system status, $F_{c.k}$ is control signal, u_k is excitation signal, e_k is residual vibration signal. Therefore, the x-LMS algorithm with state feedback shown in Figure 3b can be expressed as

$$F_{c.k} = \sum_{j=1}^{M}\sum_{i=0}^{N-1} w_{ji.k}x_{j.k-i} = \sum_{j}^{M} {w_{j.k}}^{\mathrm{T}}X_{j.k} = \sum_{j}^{M} {X_{j.k}}^{\mathrm{T}}w_{j.k}, \tag{14a}$$

$$w_{j.k+1} = w_{j.k} - 2\mu {e_k}^{\mathrm{T}} \cdot L \cdot f_{j.k}, \tag{14b}$$

$$f_{j.k} = c \cdot {XX_{j.k}}^{\mathrm{T}}, \tag{14c}$$

where

$$X_{j.k} = \left[x_{j.k} \;\; x_{j.k-1} \;\; x_{j.k-2} \cdots x_{j.k-(N-1)}\right]^{\mathrm{T}}, \tag{15a}$$

$$w_{j.k} = \left[w_{j0.k} \;\; w_{j1.k} \;\; w_{j2.k} \cdots w_{jN-1.k}\right]^{\mathrm{T}}, \tag{15b}$$

$${XX_{j.k}}^{\mathrm{T}} = \left[{X_{j.k}}^{\mathrm{T}}; {X_{j.k-1}}^{\mathrm{T}}; \cdots ; {X_{j.k-m+1}}^{\mathrm{T}}\right], \tag{15c}$$

where $X_{j.k}$ is the $N \times 1$ dimensional vector corresponding to the jth state variable of the reference signal, and $w_{j.k}$ is the $N \times 1$ dimensional tap-weight vector at time k; ${XX_{j.k}}^{\mathrm{T}}$ is the $m \times N$ matrix of the reference signal corresponding to the current and past jth state variable at time k; c is the $n \times m$ finite pulse filter corresponding to the transfer function of control channel; μ is the step factor; $f_{j.k}$ is the signal filtered by the finite pulse filter c for the reference signal corresponding to the jth state variable; L is target-weight matrix; N, M, m and n indicate the order of the x-LMS filter, the number of state parameters and the order of the finite pulse filter corresponding to the control channel respectively.

For the iterative Eqs. (14b) and (14c) of the tap-weight vector in the x-LMS algorithm with state feedback, taking system state parameter $X_{j.k}$ as reference signal, the control signal $F_{c.k}$ can be expressed as

$$F_{c.k} = [F_{c.k} \;\; F_{c.k-1} \;\; F_{c.k-2} \cdots F_{c.k-m+1}]^{\mathrm{T}}, \tag{16}$$

$$F_{c.k} = \sum_{j=1}^{M} {XX_{j.k}}^{\mathrm{T}} \cdot w_{j.k}. \tag{17}$$

The residual vibration signal e_k is the sum of the effect of excitation source p_k and the effect of active control s_k

$$e_k = p_k + s_k. \tag{18}$$

The control criterion of x-LMS algorithm with state feedback is the minimum mean square error ξ_k of the residual vibration signal, $\xi_k = E\{{e_k}^2\}$. It is treated by transient approximation in actual application, $\xi_k \approx {e_k}^2$, then

$${e_k}^2 = (p_k + s_k)^{\mathrm{T}} \cdot L \cdot (p_k + s_k). \tag{19}$$

Taking the partial derivative of Eq. (19), the tap-weight vector can be obtained

$$\Delta w_{j.k} = \frac{\partial {e_k}^2}{\partial w_j} = 2{e_k}^{\mathrm{T}} \cdot L \cdot f_{j.k}, \tag{20}$$

$$w_{j.k+1} = w_{j.k} - \mu\Delta w_{j.k} = w_{j.k} - 2\mu {e_k}^{\mathrm{T}} \cdot L \cdot f_{j.k}. \tag{21}$$

Based on Eq. (19), it can be seen that e_k is an $n \times 1$ dimensional vector, so x-LMS algorithm with state feedback is a multi-objective control algorithm, which realizes the coordination and synthesis of different control objectives through the selection of the weight matrix L. Based on Eqs. (20) and (21), it can be found that the filtering process of each state variable and the iteration of the corresponding tap-weight vector run independently in x-LMS algorithm with state feedback. When the number of system state variables is large and the filter order is high, the calculation amount and data storage of the system will increase, thereby reducing the calculation efficiency. For this reason, the state vector can be preprocessed by using the $1 \times M$ dimensional weight vector S to simplify the calculation. This simplified processing will be applied to the control of the active mounting system in the section 5. In order to achieve a faster convergence rate, the normalization method is applied [33]

$$w_{j.k+1} = w_{j.k} - \frac{\lambda {e_k}^{\mathrm{T}} \cdot L \cdot f_{j.k}}{\gamma + {f_{j.k}}^{\mathrm{T}} \cdot f_{j.k}}, \tag{22}$$

where λ is a fixed convergence factor; γ is a control factor to prevent ${f_{j.k}}^{\mathrm{T}} \cdot f_{j.k}$ from being too small.

4.2 System Controller Based on *x*-LMS Algorithm with State Feedback

In the application of x-LMS algorithm with state feedback, detecting the state variables of the system is the first step. However in the actual mounting system, the state variables of the system are not all measurable, so a state observer or filter is needed to estimate the system

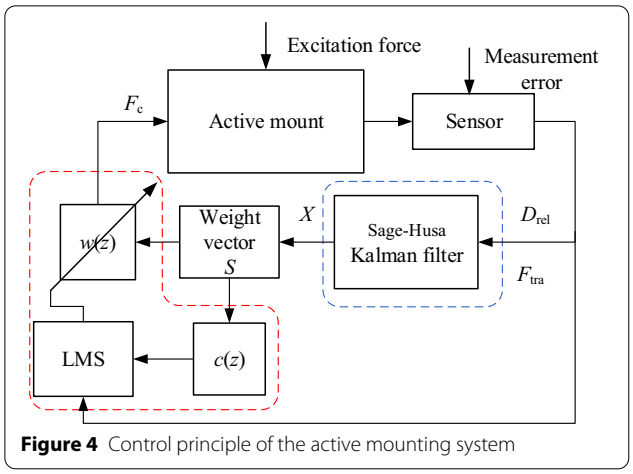

Figure 4 Control principle of the active mounting system

state, the corresponding control principle of the active mounting system is shown in Figure 4.

Because the engine excitation force in the active mounting system is related to the engine speed, that is, the variance matrix Q of the excitation signal is time-varying. Therefore, the Sage-Husa Kalman filter is explored to realize the state estimation of the system when the statistical characteristics of the excitation signal are time-varying.

First, the state Eq. (1) of the active mounting system is discretized:

$$X_k = GX_{k-1} + H_1F_{c.k-1} + H_2F_{in.k-1}, \tag{23a}$$

$$e_k = CX_k + DF_{c.k} + \eta_k \tag{23b}$$

$$\begin{aligned} G &= \mathrm{expm}(AT), \\ H_1 &= A^{-1}\cdot(G - I_\mathrm{M})\cdot B_1, \\ H_2 &= A^{-1}\cdot(G - I_\mathrm{M})\cdot B_2, \end{aligned} \tag{23c}$$

where expm(·) is the matrix index; I_M is the identity matrix. Based on the measured relative displacement and transmitted force of the active mount as input, the Sage-Husa Kalman filter [34] can be expressed as

$$P_{k/k-1} = GP_{k-1}G^\mathrm{T} + H_2\widehat{Q}_{k-1}H_2^\mathrm{T}, \tag{24a}$$

$$\widehat{X}_{k,k-1} = G\widehat{X}_{k-1} + H_1F_{c.k-1} + H_2\widehat{q}_{k-1}, \tag{24b}$$

$$v_k = e(k) - C\widehat{X}_{k,k-1} - DF_{c.k} - r_k, \tag{24c}$$

$$K_k = P_{k/k-1}C^\mathrm{T}\left[CP_{k/k-1}C^\mathrm{T} + R_k\right]^{-1}, \tag{24d}$$

$$P_k = (I_\mathrm{M} - K_kC)P_{k/k-1}(I_\mathrm{M} - K_kC)^\mathrm{T} + K_kR_kK_k{}^\mathrm{T}, \tag{24e}$$

$$\widehat{X}_k = \widehat{X}_{k-1} + K_k\cdot v_k, \tag{24f}$$

$$\widehat{q}_k = (1-d_k)\widehat{q}_{k-1} + d_k\left[H_2^\mathrm{T}H_2\right]^{-1}H_2^\mathrm{T}\left(\widehat{X}_k - G\widehat{X}_{k-1} - H_1F_{c.k-1}\right), \tag{24g}$$

$$\begin{aligned} \widehat{Q}_k =& (1-d_k)\widehat{Q}_{k-1} + d_k\left[H_2^\mathrm{T}H_2\right]^{-1} \\ & H_2^\mathrm{T}\left(K_kv_kv_k{}^\mathrm{T}K_k{}^\mathrm{T} + P_k - GP_{k-1}G^\mathrm{T}\right) \\ & H_2\left[H_2^\mathrm{T}H_2\right]^{-1}, \end{aligned} \tag{24h}$$

$$d_k = (1-b)/\left(1-b^{k+1}\right), \tag{24i}$$

where $E[F_{in.k-1}] = q_{k-1}$; $E[\eta_k] = r_k$; $cov\left[F_{in.k}, F_{in.j}\right] = Q_k$; $cov\left[\eta_k, \eta_j\right] = R_k$; forgetting factor $b \in (0, 1)$; $\widehat{X}_k$ is the estimate of system state X_k; based on $\widehat{X}_k$, $F_{c.k}$ can be obtained by discretizing Eq. (12)

$$\begin{aligned} F_{c.k} =& (E^HA_\mathrm{T}d\frac{nI_k}{l_\mathrm{T}} - k_\mathrm{a}\frac{\widehat{X}_{1.k} - \widehat{X}_{3.k}}{K_\mathrm{amp}} - b_\mathrm{T}\frac{\widehat{X}_{2.k} - \widehat{X}_{4.k}}{K_\mathrm{amp}} \\ & - m_\mathrm{a}\frac{(\widehat{X}_{2.k} - \widehat{X}_{2.k-1}) - (\widehat{X}_{4.k} - \widehat{X}_{4.k-1})}{\Delta tK_\mathrm{amp}} - \sigma_\mathrm{p}A_\mathrm{T} - F_\mathrm{r})/K_\mathrm{amp}. \end{aligned} \tag{25}$$

Combining Eqs. (14) and (25), the control current I_k of the MA can be given by

$$I_k = \frac{\left(K_\mathrm{amp}\sum_j^M \widehat{X}_{j.k}^\mathrm{T}w_{j.k} + k_\mathrm{a}\frac{\widehat{X}_{1.k}-\widehat{X}_{3.k}}{K_\mathrm{amp}} + b_\mathrm{T}\frac{\widehat{X}_{2.k}-\widehat{X}_{4.k}}{K_\mathrm{amp}} + m_\mathrm{a}\frac{(\widehat{X}_{2.k}-\widehat{X}_{2.k-1})-(\widehat{X}_{4.k}-\widehat{X}_{4.k-1})}{\Delta tK_\mathrm{amp}} + \sigma_\mathrm{p}A_\mathrm{T} + F_\mathrm{r}\right)l_\mathrm{T}}{nE^HA_\mathrm{T}d}. \tag{26}$$

5 Validation

In order to verify the effectiveness of the designed controller, simulation based on a MA is designed, which is divided into two parts: (i) Dynamic force test of the MA in blocked state; (ii) A simulation model of a two-degree-of-freedom active mounting system is established, and the simulation is carried out with the output force of the MA as input.

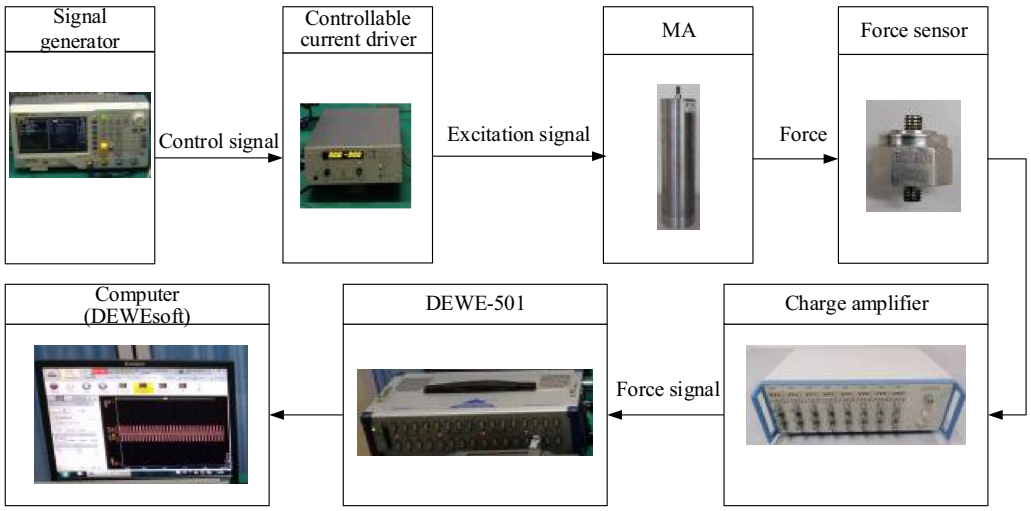

Figure 5 Dynamic force experiment platform of the MA

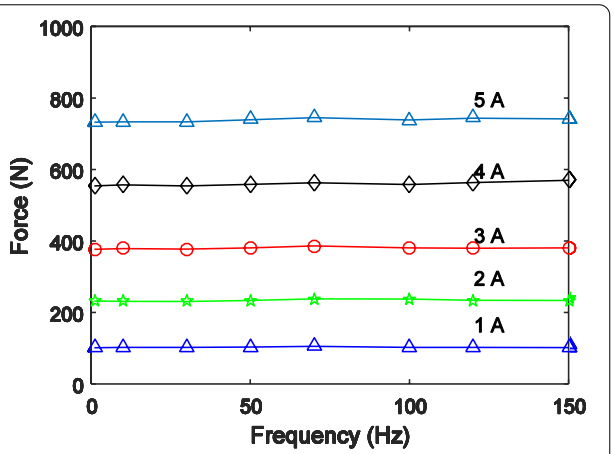

Figure 6 Dynamic force test results of the MA

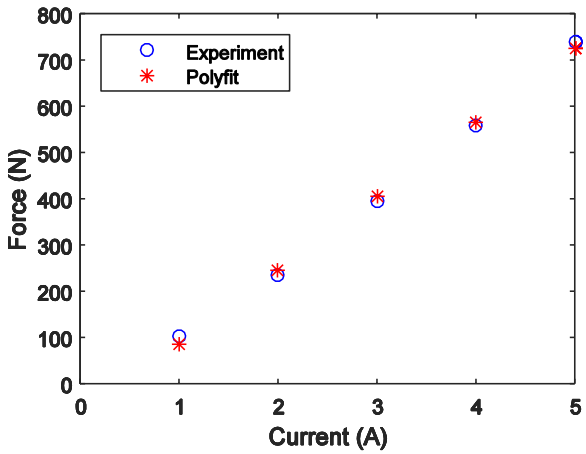

Figure 7 Output force-current relationship of the MA

Table 1 The maximal variation E_{max} and relative variation $E_{relative}$ of the output force amplitude under different frequencies

	1 A	2 A	3A	4 A	5A
E_{max} (N)	3.91	7.43	9.44	15.91	13.23
$E_{relative}$ (%)	3.81	3.17	2.48	2.84	1.79

5.1 Dynamic Force Test of the MA

Figure 5 shows the established experimental platform for dynamic force test of the MA. The core component of the MA is a Terfenol-D rod with a length of 79.6 mm and a diameter of 20 mm. The signal generator generates the control signal, which is amplified by the controllable current driver to generate the excitation current to the MA. The output force of the MA is measured by a piezoelectric force sensor (model: BZ1201). The signal of the piezoelectric sensor is conditioned by the charge amplifier, and then is collected by the data acquisition system (Type: DEWE-501).

Figure 6 presents the experimental tests in profile of the amplitudes of output force versus frequency, when the MA is under harmonic input with different amplitudes (1–5 A with interval of 1 A) and 8 kinds of different frequencies (1, 10, 30, 50, 70, 100, 120, 150 Hz) under the blocked condition. It can be seen from Figure 6 that the output force amplitude of the MA varies little under a certain amplitude of the excitation current. In order to show its variation more clearly, the maximal variation E_{max} and relative variation $E_{relative}$ of the output force

Table 2 Parameters of two-degree-of-freedom active mounting system

Parameter	Value
1/4 engine mass m_e (kg)	50
1/4 sprung mass m_b (kg)	300
Rubber spring stiffness k_m (kN/m)	180
Rubber spring damping b_m (N·s/m)	50
Suspension stiffness k_s (kN/m)	16
Suspension damping b_s (N·s/m)	1000
Sampling interval T (s)	1×10^{-3}
Target weight matrix L	[10000 0; 0 1]
Preprocessing weight matrix S	[1 1 −1 −1]
Mean of measurement noise $\boldsymbol{r_k}$	[0; 0]
Variance matrix of measure noise $\boldsymbol{R_k}$	$[2\times10^{-15}\ 0; 0\ 5\times10^{-6}]$
Fixed convergence factor $\boldsymbol{\lambda}$	7×10^{-4}
Control factor $\boldsymbol{\gamma}$	1×10^{-4}
Forgetting factor $\boldsymbol{b}$	0.99
LMS filter order N	32

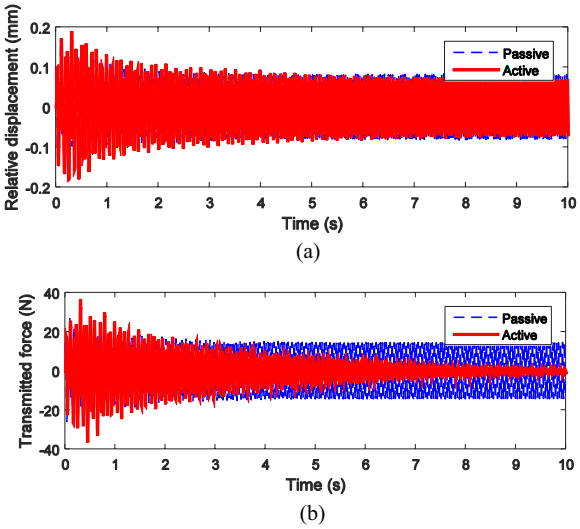

Figure 8 Comparison results of active mount and passive mount at the engine speed of 750 r/min: **a** the relative displacement and **b** the transmitted force

amplitude under different frequencies are calculated respectively. The results are shown in Table 1.

$$E_{\max} = \max\left(F_{\mathrm{T},i}\right) - \min\left(F_{\mathrm{T},i}\right), i = 1, 2, \cdots, 8, \quad (27)$$

$$E_{\mathrm{relative}} = \frac{E_{\max}}{\frac{1}{n}\sum_{i=1}^{n} F_{\mathrm{T},i}}, n = 8. \quad (28)$$

where $F_{\mathrm{T},i}$ represents the output force amplitude of the MA excitation current at a certain amplitude (1–5 A, with an interval of 1 A) of the excitation current at the ith frequency.

It can be seen from Table 1, compared to other amplitudes of the excitation currents, $E_{\max}$ is the largest when the excitation current is 4 A, and E_{relative} is the largest when the excitation current is 1 A.

Figure 7 shows the relationship between the output force of the MA (average value at 8 frequencies) and the excitation current, which has been linearly fitted. And the relationship between the fitted output force and the excitation current is expressed as Eq. (29). It can be seen from Figure 7 that the experimental results and the fitting results are agreed well.

$$F_{\mathrm{T}} = 159.7312 I_{\mathrm{amp}} - 73.5026, \quad (29)$$

where I_{amp} indicates the amplitude of the excitation current.

5.2 Simulation of Two-Degree-of-Freedom Active Mounting System

The establishment of a simulation model in MATLAB/Simulink mainly includes two parts: One part is the model of the HAM. Its gain K_{amp} depends on the stroke of the MA and the relative displacement between the engine and the sprung mass. According to Refs. [35–37], it is assumed that the maximum value of the relative displacement between the engine and the sprung mass is 0.4 mm, and the free stroke of the MA in Section 5.1 is ±50 μm, so take $K_{\mathrm{amp}} = 8$. The other part is the model of the two-degree-of-freedom active mounting system, which is established using Eqs. (14), (22), (23) and (24) based on the derived x-LMS algorithm with state feedback and Sage-Husa Kalman filter. The parameters of the model of the two-degree-of-freedom active mounting system are shown in Table 2. Basic working principle of the simulation is as follows: the MATLAB/Simulink simulation model runs on the PC-based platform, which outputs a control signal to a controllable current driver to apply the excitation current to the MA, and receives the output force of the MA as the input of the simulation model through a force sensor and a charge amplifier.

In the simulation platform, a four-cylinder four-stroke engine is taken as excitation source. The vertical excitation force of 1/4 engine is expressed as second-order inertial force, which can be expressed as [37]

$$F_{\text{in}} = m_{\text{c}}\tau\sigma\omega^2\cos 2\omega t, \tag{30}$$

where m_{c} is the mass of the reciprocating part of the cylinder piston; τ is the crank radius; σ is the ratio of crank radius to connecting rod length; ω is the rotational angular frequency corresponding to different engine speeds.

5.2.1 Simulation Results at Steady State (Constant Engine Speed)

In order to verify the effectiveness of the proposed control method under constant engine speed (steady state) conditions, two engine speeds of 750 r/min (idling speed) and 3000 r/min are selected for steady-state simulation. Figure 8 shows the comparison between the results of the vibration isolation effect (transmitted force) and relative displacement response of the active mount and those of the passive mount at the engine speed of 750 r/min. Figure 8a shows the comparison between the results of active mount and those of the passive mount in profiles of the relative displacement versus time. It can be seen from Figure 8a that since the relative displacement of the passive mount has reached a small value, the improvement of the relative displacement of the active mount is not obvious, which is by 11.37%, compared with the passive mount. Figure 8b shows the comparison between the results of active mount and those of the passive mount in profiles of the transmitted force versus time. It can be seen from Figure 8b that compared with the passive mount, the transmitted force of the active mount is reduced significantly, which is by 86.17%. At the beginning of the simulation, due to the unstable state of the system and a certain number of iterations for the tap-weight vector $w_{.k}$, the results of the active mount are not ideal. However, as the simulation time increases, the transmitted force of the active mount gradually decreases.

Figure 9 shows the comparison between the estimated system state and the real system state at the engine speed of 750 r/min. Figure 9a is the comparison between the estimated result and the actual result of engine displacement. It can be seen from the Figure 9a that the Sage-Husa Kalman filter can realize the estimation of the engine displacement at the engine speed of 750 r/min. Figure 9b (engine velocity), Figure 9c (sprung mass displacement), Figure 9d (sprung mass velocity) show the similar results.

Figure 10 shows the comparison between the results of the vibration isolation effect (transmitted force) and relative displacement response of the active mount and those of the passive mount at the engine speed of 3000 r/min, which is similar to the results at the engine speed of 750 r/min. It can be seen from Figure 10 that compared with the passive mount, the relative displacement and the

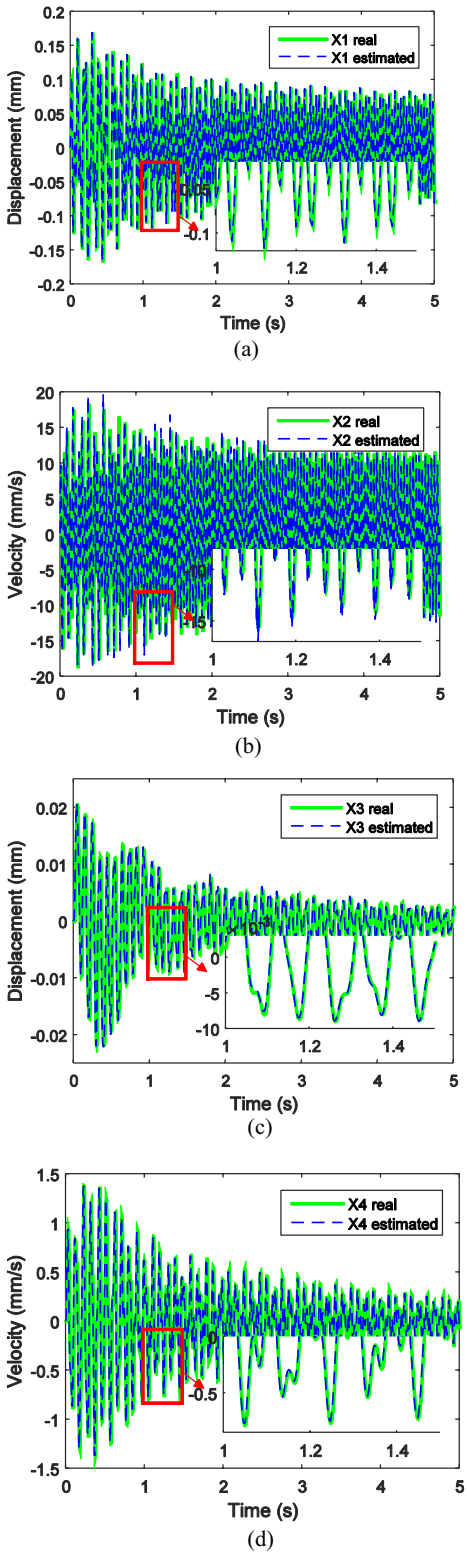

Figure 9 Comparison between estimated system state and real system state at the engine speed of 750 r/min: **a** X_1: engine displacement, **b** X_2: engine velocity, **c** X_3: sprung mass displacement, and **d** X_4: sprung mass velocity

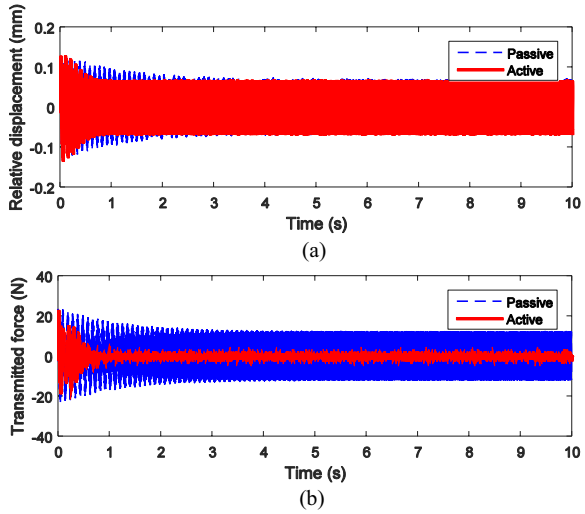

Figure 10 Comparison results of active mount and passive mount at the engine speed of 3000 r/min: **a** the relative displacement and **b** the transmitted force

transmitted force of the active mount is reduced by 1.06% and 98.24% respectively. But compared with the results at the engine speed of 750 r/min, the relative displacement and transmitted force of the active mount can stabilize faster at the engine speed of 3000 r/min.

Figure 11 shows the comparison between the estimated system state and the actual system state at the engine speed of 3000 r/min. It can be seen from the Figure 11a and b that the Sage-Husa Kalman filter can realize the estimation of the engine displacement and engine velocity at the engine speed of 3000 r/min. It can be seen from the Figure 11c and d that it is impossible to estimate the sprung mass displacement and sprung mass velocity, the values of which are in the same order of magnitude as the measurement error. But due to their extremely small values, their contribution to the control effect of x-LMS algorithm with state feedback can be ignored. In summary, the proposed control method of the active mount can effectively improve the transmitted force, while ensuring the relative displacement of the active mount under constant engine speed (steady state) conditions.

5.2.2 Simulation Results at Dynamic State (Variable Engine Speed)

In order to verify the effectiveness of the proposed control method under variable engine speed (dynamic state) condition, the dynamic simulation is conducted when the engine speed increase from 750 r/min to 2100 r/min. Specifically the engine speed increases from 750 r/min to 2100 r/min at a constant rate and then remains stable as shown in Figure 12. Figure 13 shows the comparison

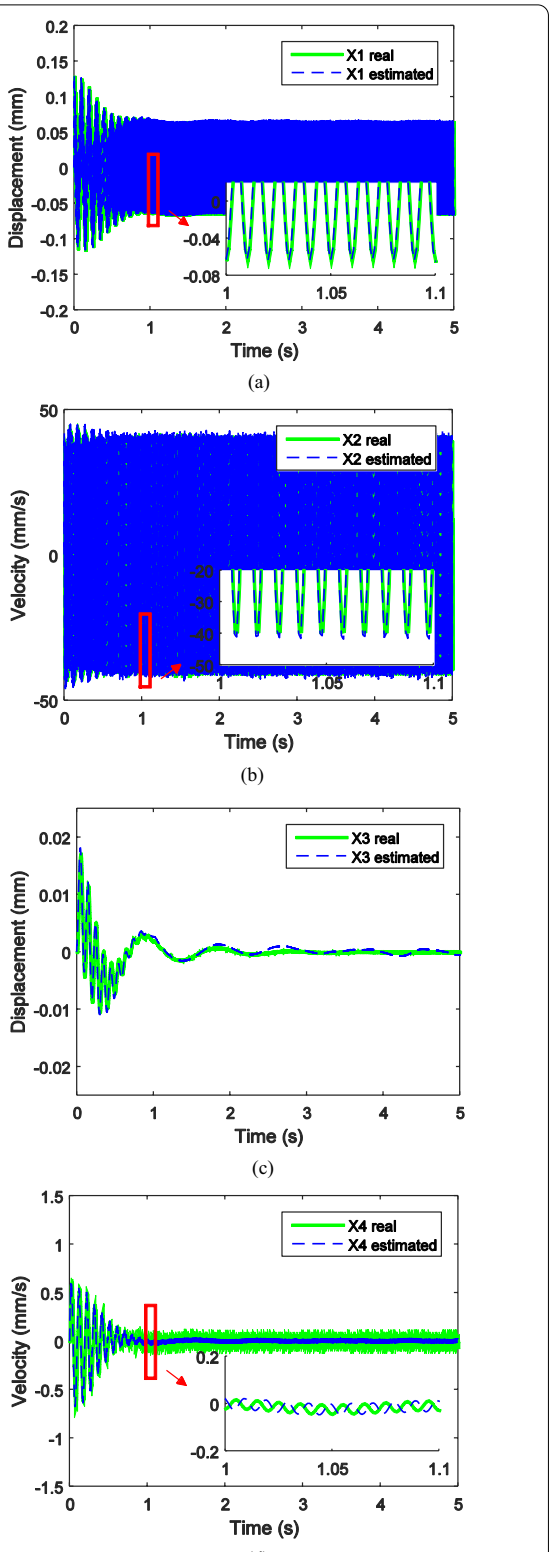

Figure 11 Comparison between estimated system state and real system state at the engine speed of 3000 r/min: **a** X_1: engine displacement, **b** X_2: engine velocity, **c** X_3: sprung mass displacement, and **d** X_4: sprung mass velocity

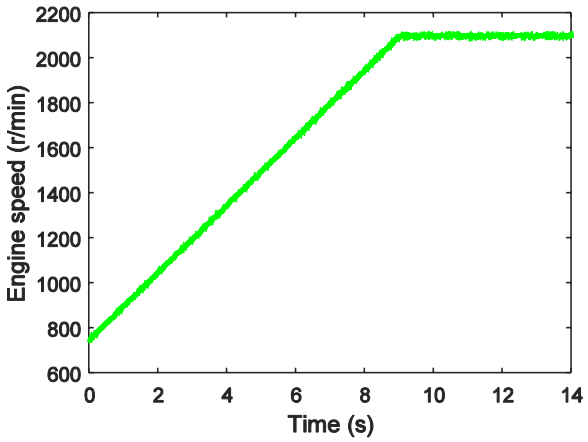

Figure 12 The process of variable engine speed

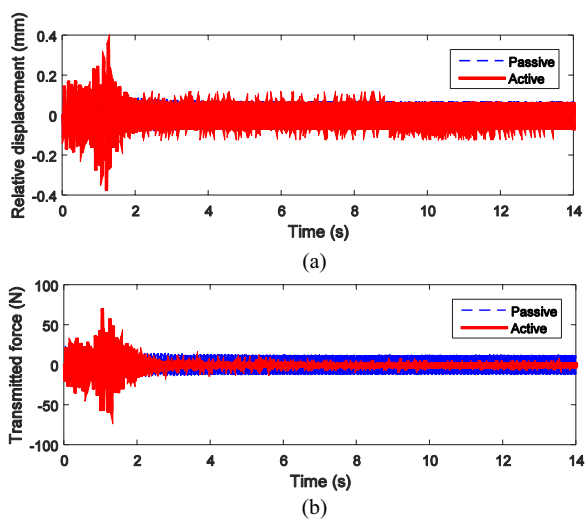

Figure 13 Comparison results of active mount and passive mount under variable engine speed conditions (engine speed increased from 750 r/min to 2100 r/min): **a** the relative displacement and **b** the transmitted force

between the results of the vibration isolation effect (transmitted force) and relative displacement response of the active mount and those of the passive mount under variable engine speed condition. Figure 13a shows the comparison between the results of the active mount and those of the passive mount in profiles of the relative displacement versus time. It can be seen from Figure 13a that the relative displacement of the active mount is reduced by 2.00% compared with the passive mount, but the relative displacement of the active mount increases at some moments compared to steady state due to the unstable state of the system and computation of the tap-weight vector $w_{.k}$ at variable engine speed. Figure 13b shows the comparison between the results of the active mount and those of the passive mount in profiles of the transmitted force versus time. It can be seen from Figure 13b that compared with the passive mount, the transmitted force of the active mount is reduced significantly, which is by 96.96%. At the beginning of the simulation, due to the unstable state of the system and a certain number of iterations for the tap-weight vector $w_{.k}$, the results of the active mount are not ideal. However, as the simulation time increases, the transmitted force of the active mount gradually decreases.

Figure 14 shows the comparison between the estimated system state and the real system state under variable engine speed condition. Figure 14a is the comparison between the estimated result and the actual result of engine displacement. It can be seen from the Figure 14a that the Sage-Husa Kalman filter can realize the estimation of the engine displacement under variable engine speed condition. Figure 14b (engine velocity), Figure 14c (sprung mass displacement), Figure 14d (sprung mass velocity) show the similar results.

6 Conclusions

In this paper, an active mount based on MA was proposed, which mainly includes three parts: rubber spring, MA, and HAM. The rubber spring supports the engine weight, playing the role of the passive mount. The MA outputs controlled force. The HAM amplifies the output displacement of the MA, transmits the output force from the MA to the engine, and alleviates the impact on the MA during the engine vibration. Then the dynamic model of the proposed active mount was established.

Based on the principle of x-LMS algorithm, a control method of x-LMS algorithm with the system state as the reference signal was proposed to address the problem of the dependent on the excitation signal in the x-LMS algorithm. In application of the proposed control method, to address the problem of unmeasurable state of the active mounting system, the Sage-Husa Kalman filter was explored to realize the state estimation of the active system since the statistical characteristics of the excitation signal are time-varying.

In order to verify the feasibility and capability of the proposed control method, the simulation of a two-degree-of-freedom active mounting system model was carried out. Firstly, the dynamic force test of the MA was conducted. The experimental results shows that the output force amplitude of the MA varies little with a certain amplitude of the excitation current at different frequencies, and the output force amplitude has a linear relationship with the excitation current. Secondly, a simulation based on the established model of a

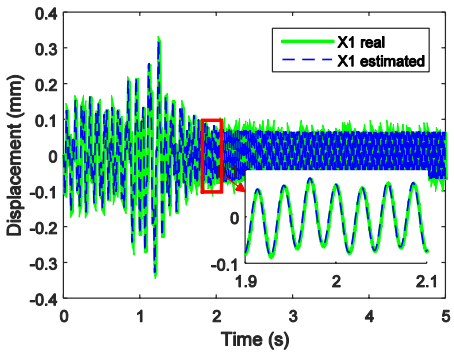

Figure 14 Comparison between estimated system state and real system state under variable engine speed condition (engine speed increased from 750 r/min to 2100 r/min): **a** X_1: engine displacement, **b** X_2: engine velocity, **c** X_3: sprung mass displacement, and **d** X_4: sprung mass velocity

two-degree-of-freedom active mounting system was carried out with the output force of the MA as the input.

The working conditions of the simulation includes steady state (constant engine speed: 750 r/min and 3000 r/min) and dynamic state (variable engine speed: 750 r/min increased to 2100 r/min). Under constant engine speed (steady state) conditions, the relative displacement and transmitted force of the active mount are reduced by 11.37% and 86.17% (750 r/min), 1.06% and 98.24% (3000 r/min) compared with the passive mount. Under variable engine speed (dynamic state) condition, the relative displacement and transmitted force of the active mount are reduced by 2.00% and 96.96% compared with the passive mount. The simulation results show that the Sage-Husa Kalman filter can realize the estimation of the system state under different conditions, and the x-LMS algorithm with state feedback can effectively reduce the transmitted force of the active mount while ensuring the relative displacement of the active mount.

Acknowledgements
The authors would like to thank to Mr. Yang Liu and Mr. Zengcheng Liao, graduate students from Hefei University of Technology, China, for their assistance in experimental tests.

Authors' contributions
ZS contributed the experimental work, theoretical work and original draft of the paper. XB contributed theoretical work and the review and editing of the paper. LQ contributed he experimental work and supervision of the whole work. PC contributed theoretical work and simulation work. AZ contributed the experimental results processing and revised the paper. All authors read and approved the final manuscript.

Authors' Information
Zhiyuan Si, born in 1982, is currently a PhD candidate at *Hefei University of Technology, China*. He received his master degree in vehicle engineering from *Beihang University, China*, in 2009. His research interests include modeling and control of nonlinear behavior of smart materials and their application in vehicle engineering.
Xianxu 'Frank' Bai, born in 1984, is currently an professor at *Hefei University of Technology, China*. He received his Ph.D. degree in Instrument Science and Technology from *Chongqing University, China*, in 2013. His research interests include two areas: (i) Design, optimization, dynamics, and control of smart structures systems based on smart materials, including magnetorheological fluids/elastomers and magnetostrictive materials, applied to automotive systems; and (ii) new mechatronics-based vehicle dynamics and control with emphasis on intelligent/unmanned vehicles. Currently, Dr. Bai serves as an associate editor of *Journal of Intelligent Material Systems and Structures* and *SAE International Journal of Connected and Automated Vehicles*.
Lijun Qian, born in 1962, is currently a professor and a PhD candidate supervisor at *Hefei University of Technology, China*. He received his Ph.D. degree in

vehicle engineering from *Hefei University of Technology, China*, in 2004. His research interests include vehicle system dynamics, hybrid electric vehicles, and active automotive safety.
Peng Chen, born in 1991, is currently an engineer at *Guangzhou Automobile Research and Design Center, China*. He received his Ph.D. degree in vehicle engineering from *Hefei University of Technology, China*, in 2018. His research interests are the modeling and control of nonlinear behavior of smart materials and their application in vibration control.

Funding
Supported by National Natural Science Foundation of China (Grant No. 52272392) and Fundamental Research Funds for the Central Universities of China (Grant No. JD2019JGPY0018).

Competing interests
The authors declare no competing financial interests.

Author Details
[1]Laboratory for Adaptive Structures and Intelligent Systems (LASIS), Department of Vehicle Engineering, Hefei University of Technology, Hefei 230009, China. [2]School of Mechanical Engineering, Anhui Science and Technology University, Fengyang 233100, China. [3]Guangzhou Automobile Research and Design Center, Guangzhou 511434, China.

Received: 25 October 2022 Revised: 25 October 2022 Accepted: 31 October 2022
Published online: 07 December 2022

References

[1] H Zhou, H Liu, P Gao, et al. Optimization design and performance analysis of vehicle powertrain mounting system. *Chinese Journal of Mechanical Engineering*, 2018, 31:31. https://doi.org/10.1186/s10033-018-0237-2.
[2] T M Nguyen, C Ciocanel, M H Elahinia. A squeeze-flow mode magnetorheological mount: Design, modeling, and experimental evaluation. *Journal of Vibration and Acoustics*, 2012, 134(2). https://doi.org/10.1115/1.4005011.
[3] Y Zhang, J Zhang, W Shangguan, et al. Modeling and experimental study of a passive hydraulic engine mount with inertia and direct-decoupler. *Chinese Journal of Mechanical Engineering*, 2008, 21(3): 31-35. https://doi.org/10.3901/CJME.2008.03.031.
[4] J Hu, W Chen, H Huang. Decoupling analysis for a powertrain mounting system with a combination of hydraulic mounts. *Chinese Journal of Mechanical Engineering*, 2013, 26(4): 737-745. https://doi.org/10.3901/CJME.2013.04.737.
[5] H Zhang, W Shi, J Ke, et al. A review on model and control of electromagnetic active engine mounts. *Shock and Vibration*, 2020(5): 1-20. https://doi.org/10.1155/2020/4289281.
[6] X X Bai, F L Cai, P Chen. Resistor-capacitor (RC) operator-based hysteresis model for magnetorheological (MR) dampers. *Mechanical Systems and Signal Processing*, 2019, 117: 157-169. https://doi.org/10.1016/j.ymssp.2018.07.050.
[7] S Chakrabarti, M J Dapino. Hydraulically amplified Terfenol-D actuator for adaptive powertrain mounts. *Journal of Vibration and Acoustics*, 2011, 133(6). https://doi.org/10.1115/1.4004669.
[8] Y M Han, S M Choi, S B Choi, et al. Design and control of a hybrid mount featuring a magnetorheological fluid and a piezostack. *Smart Materials and Structures*, 2011, 20(7): 075019. https://doi.org/10.1088/0964-1726/20/7/075019.
[9] A J Hillis. Multi-input multi-output control of an automotive active engine mounting system. *Proceedings of the Institution of Mechanical Engineers, Part D: Journal of Automobile Engineering*, 2011, 225(11): 1492-1504. https://doi.org/10.1177/0954407011407701.
[10] R Kraus, S Herold, J Millitzer, et al. Development of active engine mounts based on piezo actuators. *ATZ Worldwide*, 2014, 116(1): 46-51. https://doi.org/10.1007/s38311-014-0012-7.
[11] B H Lee, C W Lee. Model based feed-forward control of electromagnetic type active control engine-mount system. *Journal of Sound and Vibration*, 2009, 323(3-5): 574-593. https://doi.org/10.1016/j.jsv.2009.01.033.
[12] R Li, W M Chen, C R Liao. Hierarchical fuzzy control for engine isolation via magnetorheological fluid mounts. *Proceedings of the Institution of Mechanical Engineers, Part D: Journal of Automobile Engineering*, 2010, 224(2): 175-187. https://doi.org/10.1243/09544070JAUTO1246.
[13] D X Phu, S B Choi. Vibration control of a ship engine system using high-load magnetorheological mounts associated with a new indirect fuzzy sliding mode controller. *Smart Materials and Structures*, 2015, 24(2). https://doi.org/10.1088/0964-1726/24/2/025009.
[14] F Hausberg, M Plochl, M Rupp, et al. Combination of map-based and adaptive feedforward control algorithms for active engine mounts. *Journal of Vibration and Control*, 2017, 23(19): 3092-3107. https://doi.org/10.1177/1077546315626323.
[15] S H Kim, U H Park, J H Kim. Voice coil actuated (VCA) engine mount for vibration reduction in automobile. *International Journal of Automotive Technology*, 2020, 21(3): 771-777. https://doi.org/10.1007/s12239-020-0075-y.
[16] Y H Shin, S J Moon, W J Jung, et al. Experimental approach to active mounts using electromagnetic actuator and rubber with consideration of shock resistance for naval shipboard equipment. *Shock and Vibration*, 2019, https://doi.org/10.1155/2019/3958359.
[17] F L Xin, X X Bai, L J Qian. Principle, modeling, and control of a magnetorheological elastomer dynamic vibration absorber for powertrain mount systems of automobiles. *Journal of Intelligent Material Systems & Structures*, 2017, 28(16): 2239-2254. https://doi.org/10.1177/1045389X16672731.
[18] T Ushijima, S Kumakawa. Active engine mount with piezo-actuator for vibration control. *SAE Technical Papers*, 1993, https://doi.org/10.4271/930201.
[19] Z Deng, M J Dapino. Review of magnetostrictive materials for structural vibration control. *Smart Materials and Structures*, 2018, 27(11): 113001. https://doi.org/10.1088/1361-665X/aadff5.
[20] C Niezrecki, D Brei, S Balakrishnan, et al. Piezoelectric actuation: state of the art. *Shock and Vibration Digest*, 2001, 33(4): 269-280. https://doi.org/10.1177/058310240103300401.
[21] H X Yang, R M Wang, D M Liu. A study on active engine vibration control by applying hydraulic-piezoelectric mount. *Advanced Materials Research*, 2013, 721: 501-504. https://doi.org/10.4028/www.scientific.net/AMR.721.501.
[22] Y T Choi, N M Wereley, G J Hiemenz. Frequency shaped semi-active control for magnetorheological fluid-based vibration control systems. *ASME Conference on Smart Materials*, 2013, https://doi.org/10.1115/SMASIS2013-3268.
[23] S Wang, M Elahinia. Displacement and force control of a quarter car using a mixed mode MR mount. *Shock and Vibration*, 2013, 20(1): 1-17. https://doi.org/10.3233/SAV-2012-0721.
[24] A M M Mahil, W F Faris. Modelling and control of four and six DOF active engine mount system using (PID and LQR). *International Journal of Vehicle Noise and Vibration*, 2014, 10(4): 326. https://doi.org/10.1504/IJVNV.2014.065640.
[25] X Zhang, H Zhang, M Ahmadian, et al. Study on squeeze mode magneto-rheological engine mount with robust h-infinite control. *SAE Technical Papers*, 2011, https://doi.org/10.4271/2011-01-0757.
[26] S S Hosseini, J Marzbanrad. Robust H∞ controller in a MRF Engine Mount for improving the vehicle ride comfort. *International Journal of Acoustics and Vibration*, 2020, 25(2): 219-225. https://doi.org/10.20855/ijav.2020.25.21592.
[27] J Yu, Z Jiao, S Wu. Design and simulation study on new servo valve direct driven by piezoelectric actuator using hydraulic amplification. *Journal of Mechanical Engineering*, 2013, 49(2): 151-158. (in Chinese) https://doi.org/10.3901/JME.2013.02.151.
[28] F Braghin, S Cinquemani, F Resta. A model of magnetostrictive actuators for active vibration control. *Sensors and Actuators A-physical*, 2011, 165(2): 342-350. https://doi.org/10.1016/j.sna.2010.10.019.
[29] M D Bryant, N Wang. Audio range dynamic models and controllability of linear motion terfenol actuators. *Journal of Intelligent Material Systems and Structures*, 1994, 5(3): 431-436. https://doi.org/10.1177/1045389X9400500318.
[30] B W Wang, S Y Cao, M W Huang. *Magnetostrictive material and components*. Beijing: Metallurgy Industry Publishing Company, 2008. (in Chinese)

[31] V Apicella, C S Clemente, D Davino, et al. Review of modeling and control of magnetostrictive actuators. *Actuators*, 2019, 8(2): 45. https://doi.org/10.3390/act8020045.
[32] H Olsson, K J Astrom, C C De Wit, et al. Friction models and friction compensation. *European Journal of Control*, 1998, 4(3): 176-195. https://doi.org/10.1016/S0947-3580(98)70113-X.
[33] S S Haykin. *Adaptive filter theory*. India: Pearson Education, 2007.
[34] C Olsson. Active automotive engine vibration isolation using feedback control. *Journal of Sound and Vibration*, 2006, 294(1-2): 162-176. https://doi.org/10.1016/j.jsv.2005.10.022.
[35] J G Holt, M D Rao, J R Blough, et al. Time history-based excitation in the dynamic characterization of automotive elastomers. *Proceedings of the Institution of Mechanical Engineers, Part D: Journal of Automobile Engineering*, 2007, 221(3): 271-284. https://doi.org/10.1243/09544070JAUTO339.
[36] R Guo, X K Wei, S Q Zhou, et al. Parametric identification study of an active engine mount: combination of finite element analysis and experiment. *Proceedings of the Institution of Mechanical Engineers Part D Journal of Automobile Engineering*, 2019, 233(2): 427-439. https://doi.org/10.1177/0954407017745748.
[37] A R Ohadi, G Maghsoodi. Simulation of engine vibration on nonlinear hydraulic engine mounts. *Journal of Vibration and Acoustics*, 2007, 129(4): 417-424. https://doi.org/10.1115/1.2748459.